Environmental Science Processes & Impacts

ROYAL SOCIETY OF CHEMISTRY

PAPER

View Article Online
View Journal

Cite this: DOI: 10.1039/d5em00847f

Sorption and desorption of per- and polyfluoroalkyl substances (PFASs) on unmodified iron oxide and silica clay minerals

Susannah Powell,[a] Hongyi Ban,[ac] Yi Sang,[a] Daewon Kim,[b] Phillip J. Milner,[b] Matthew Reid[a] and Damian E. Helbling *[a]

The goals of this study were to measure sorption kinetics, solid–water partitioning ($\log K_d$ values) as a function of pH, and percent desorption for a diverse set of PFASs on four highly abundant soil and aquifer minerals. We found that PFAS sorption was relatively fast on all four minerals and that overall $\log K_d$ values were higher for ferrihydrite and montmorillonite than for goethite and kaolinite, possibly driven by differences in surface area. We also found that $\log K_d$ values on ferrihydrite and goethite were dependent on pH levels and the length of the perfluoroalkyl chain. Significant differences in $\log K_d$ values between the iron oxide minerals were explained by differences in their respective point-of-zero-charge, and changes in PFAS speciation as a function of pH amplified those differences. Despite the relatively high $\log K_d$ values of the iron oxide minerals reflecting relatively high affinity for PFASs, facile desorption from the iron oxides suggests that PFAS sorption is driven by relatively weak electrostatic interactions. The $\log K_d$ values on montmorillonite and kaolinite were not significantly dependent on pH levels, but were dependent on the length of the perfluoroalkyl chain. Less facile desorption from the silica clay minerals suggests that PFAS sorption is driven by relatively strong hydrophobic and electrostatic interactions. Together, our data make practical contributions to support site characterization and remediation efforts, while also contributing key insights into the fundamental sorption processes.

Received 16th October 2025
Accepted 13th December 2025

DOI: 10.1039/d5em00847f

rsc.li/espi

Environmental significance

We quantified sorption kinetics, solid–water partitioning ($\log K_d$ values) as a function of pH, and the extent of desorption for a diverse set of dozens of per- and polyfluoroalkyl substances (PFASs) on two iron oxide minerals (ferrihydrite and goethite) and two silica clay minerals (montmorillonite and kaolinite). The results demonstrate that pH-dependent changes in the surface charge of the mineral and speciation of the PFASs play an important role in PFAS sorption and that iron oxide minerals exhibit relatively facile desorption when compared to silica clay minerals. Together, our data make practical contributions to support site characterization and remediation efforts, while also contributing key insights into the fundamental sorption processes.

Introduction

Per- and polyfluoroalkyl substances (PFASs) are a diverse group of persistent anthropogenic organofluorine-containing chemicals that are detected globally as environmental contaminants.[1,2] The use of PFASs in aqueous film-forming foams (AFFFs)[3–5] and consumer products that are deposited in landfills,[6,7] along with their presence in land-applied biosolids from municipal wastewater treatment plants,[8,9] results in their accumulation in soils and eventual transport onto the subsurface.[10] As a consequence, PFASs have been measured in groundwater systems around the world at concentrations ranging up to several milligrams per liter at sites adjacent to source zones.[11–13]

Once PFASs reach groundwater, their ultimate fate is determined by a number of co-occurring environmental processes. For example, PFASs can sorb to soils and aquifer minerals to varying extents based on the surface chemistry of the soils and aquifer minerals, the chemical nature of the individual PFAS, and local biogeochemical conditions including parameters such as pH, ionic strength, and the presence of other dissolved organic and inorganic substances.[14–16] PFASs that sorb under prevailing conditions will be partially sequestered near the source zone and their transport away from the source zone will be retarded as a function of their solid–water partition coefficient (K_d).[17] These types of PFASs can sustain a source zone for many years as they slowly leach away from the source zone.

[a]School of Civil and Environmental Engineering, Cornell University, Ithaca, NY, 14853, USA. E-mail: damian.helbling@cornell.edu; Fax: +1 607 255 9004; Tel: +1 607 255 5146
[b]Department of Chemistry and Chemical Biology, Cornell University, Ithaca, NY, 14853, USA
[c]Department of Chemical and Environmental Engineering, Yale University, New Haven, CT 06511, USA

PFASs that do not sorb under prevailing conditions will be transported by means of advection, diffusion, and dispersion and will migrate greater distances over shorter periods of time. These types of PFASs can impact water quality in ground water resources at distances rather far from the source zone.[18] To complicate matters further, some PFASs that sorb to soils or aquifer minerals can be (bio)transformed into PFASs that do not sorb as strongly and those PFASs can slowly leach away from the source zone for durations that are linked to the (bio)transformation kinetics.[19]

Iron oxides and silica clays are highly abundant soil and aquifer minerals that are increasingly recognized as subsurface features that strongly influence the transport and retardation of PFASs on the subsurface.[20–22] Ferrihydrite is a poorly crystalline, amorphous iron oxide mineral.[23] It is an effective sorbent due to its large surface area and mesoporous structure.[24,25] Ferrihydrite has a point-of-zero-charge (PZC) that ranges between 7.3 and 8 and is consequently a particularly effective sorbent for anions in the environment.[25,26] Goethite is a more stable, thermodynamically favorable product of ferrihydrite and other iron oxides.[27] Goethite exhibits a well-ordered crystalline structure and often forms needle-like particles that can play a significant role in controlling the mobility and retention of contaminants on the subsurface.[28] Goethite is likewise an effective sorbent but has a lower surface area and pore volume when compared to ferrihydrite. Variable coverage of surface hydroxyl groups on goethite can result in PZC values ranging between 7.5–9.5.[29–31]

Montmorillonite is a smectite phyllosilicate group clay mineral with a structure that includes two O–Si–O tetrahedral sheets sandwiching an O–Al(Mg)–O octahedral sheet,[32] with cations located in the interlayered space.[33] The sheets are linked together by van der Waals and electrostatic forces and the basal surface of the siloxane tetrahedral sheets is capable of interacting with nonpolar chemicals by means of hydrophobic interactions.[34,35] The average reported PZC for montmorillonite is 3.4 due to the presence of surface hydroxyl groups and isomorphic substitution.[36] Kaolinite is a clay mineral which features a flat plate-like structure of two basal planes, a Si–O silica tetrahedral sheet, an Al–OH gibbsite facet sheet, and edge sites that contain hydroxyl groups that can be protonated below a pH of 6–7.[37] The presence of hydroxyl groups at the basal surface of the Al–OH gibbsite facet sheet results in a hydrophilic character, while the basal surface of the Si–O silica tetrahedral sheet results in a hydrophobic character.[38] Although the positively charged edge sites may allow for some electrostatic interactions with anions, these sites are limited and kaolinite has an overall PZC of less than 4. In this context, sorption of anions is likely dominated by hydrophobic interactions.[39]

Due to the hydrophilic nature of ferrihydrite and goethite along with their reported PZC values in the range of 7.3–9.5, sorption of PFASs is expected to be driven by electrostatic interactions and H-bonding in a pH-dependent way.[40,41] Previous studies with sets of anionic perfluoroalkyl acids (PFAAs) have demonstrated that sorption on ferrihydrite and goethite can be driven by various types of electrostatic interactions including the formation of outer-sphere and inner-sphere complexes.[20,31,42] PFAS sorption on montmorillonite and kaolinite can be more complex.[43] The relatively low PZC for montmorillonite and kaolinite makes electrostatic interactions with anionic PFASs unfavorable, although the positive surface charge on the edge sites of kaolinite can support point interactions with anionic PFASs. The basal surface of the Si–O silica tetrahedral sheet of kaolinite can also support hydrophobic interactions with PFASs.

Sorption to aquifer minerals is one of the most important factors for understanding PFAS fate and transport in subsurface environments.[21] Although the sorption and desorption of certain PFASs on specific aquifer minerals including iron oxides, metal carbonates, silica clays, and organic-rich soils were previously reported, our current knowledge of PFAS sorption and desorption on aquifer minerals remains limited in scope (*i.e.*, diverse types of PFASs) and depth (*i.e.*, integrated studies of sorption and desorption as a function of pH).[44,45] The goals of this study were to measure log K_d values as a function of pH and percent desorption for a diverse set of up to 40 PFASs on four highly abundant aquifer minerals including ferrihydrite, goethite, montmorillonite, and kaolinite. The PFASs were selected to represent seven classes that were defined by their functional groups and their potential to be neutral, anionic, cationic, or zwitterionic as a function of pH. The model minerals were selected due to their relative abundance in subsurface environments and to represent sorbents that can participate in a variety of sorption mechanisms including electrostatic interactions resulting in the formation of outer-sphere or inner-sphere complexes, general hydrophobic interactions, H-bonding, and ligand exchange. By investigating the sorption of a broad range of PFASs across the four model minerals, we generated essential data to support fate and transport modelling of PFASs in subsurface environments while also contributing key insights into the fundamental sorption processes.

Materials and methods

Chemicals and reagents

We selected 40 PFASs from seven broad classes including eleven perfluoroalkyl carboxylic acids (PFCAs, C4–C14), five perfluoroalkyl sulfonic acids (PFSAs, C4, C6–C8, and C10), six fluorotelomer carboxylic acids (FTCAs, 3:3, 5:3, 7:3, 6:2, 8:2, and 10:2), three unsaturated fluorotelomer carboxylic acids (FTUCAs, 5:1:2, 7:1:2, and 9:1:2), four fluorotelomer sulfonic acids (FTSs, 4:2, 6:2, 8:2, and 10:2), two perfluoroalkyl sulfonamides (FASAs, C4 and C8), four *N*- or *N*,*N*-substituted perfluoroalkyl sulfonamides including perfluoro-*N*-(2-hydroxyethyl)-1-butanesulfonamide (FBSE), perfluoro-*N*-(2-methoxyethyl)-1-butanesulfonamide (MeFBSE), *N*-methylperfluoro-1-octanesulfonamidoacetic acid (*N*-MeFOSAA), and *N*-ethylperfluoro-1-octanesulfonamidoacetic acid (*N*-EtFOSAA), and five zwitterionic PFASs including 5:3 fluorotelomer betaine (FTB), 5:1:2 FTB, 6:2 fluorotelomer sulfonamide alkylbetaine (6:2 FTAB), *N*-(3-dimethylaminopropan-1-yl)perfluoro-1-hexanesulfonamide (AmPr-FHxSA), and *N*-[3-(perfluoro-1-hexanesulfonamido)propan-1-yl]-*N*,*N*,*N*-trimethylammonium (TAmPr-FHxSA). Each PFAS was added to one of the three PFAS

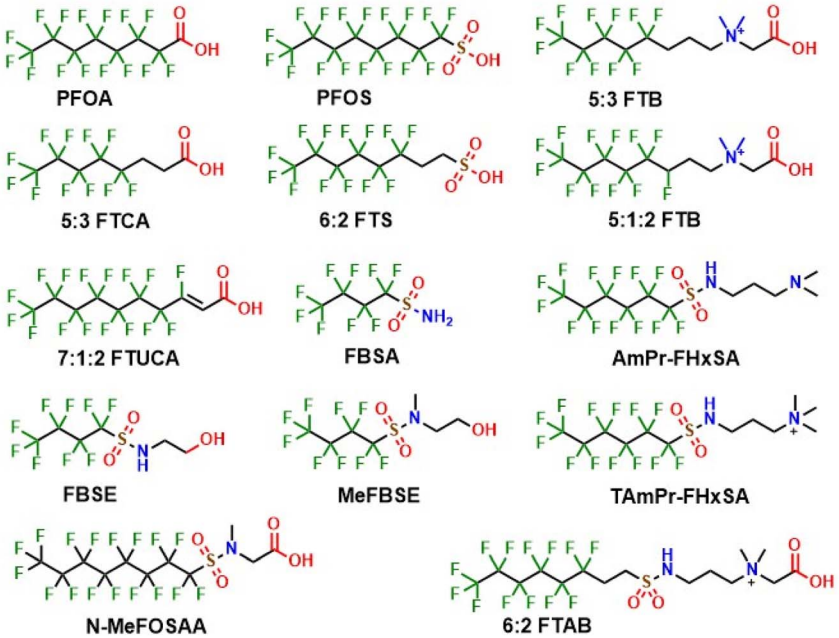

Fig. 1 Chemical structures of representative PFASs included in this study. Chemical structures are drawn as neutral molecules unless there is a cationic quaternary amine group in the structure.

stock solutions (PSSs) consisting of Milli-Q water (96%) and methanol (4%) to generate a final concentration of 0.5 mg L^{-1} for each PFAS. Chemical structures of the 14 representative PFASs are provided in Fig. 1. We used a mixture of nine isotope-labelled internal standards (ILISs, $^{13}C_4$-PFBA, $^{13}C_2$-PFHxA, $^{13}C_4$-PFOA, $^{13}C_5$-PFNA, $^{13}C_2$-PFDA, $^{13}C_2$-PFUnA, $^{13}C_2$-PFDoA, $^{18}O_2$-PFHxS, and $^{13}C_4$-PFOS) for PFAS quantification. ILISs were diluted in a mixture using Milli-Q water to yield a final concentration of 250 μg L^{-1} for each ILIS. Details on suppliers, product numbers, solvents, and stock solution concentrations are provided in Table S1 in the SI. All stock solutions and mixtures were stored at −20 °C and 4 °C, respectively, until usage. A summary of all other chemicals and solvents used in this study is provided in Table S2.

Sorbent materials

We selected four minerals for our sorption experiments. We acquired representative samples of montmorillonite K10 (Thermo Scientific), kaolinite (Sigma-Aldrich), and goethite (98% purity, Santa Cruz Biotechnology) from commercial suppliers. We also synthesized ferrihydrite according to published procedures.[24] To prepare the minerals for sorption experiments, each of the four minerals was sieved to a particle size of 10–38 μm using brass sieves (Dual Manufacturing Co.). All crushed and sieved sorbent particles were stored in glass vials at room temperature. Details of the chemical composition and physical morphology of each of the four minerals are provided in Table S3. Gas sorption measurements were conducted using nitrogen at 77 K on a Micromeritics ASAP 2460 instrument, with pressures up to 1 bar. High-purity nitrogen (99.999%) was used throughout the experiments. Prior to analysis, all samples were degassed at 100 °C for 8 h under vacuum to remove residual water and oxygen from the pores. The Brunauer, Emmett, and Teller (BET) surface area was determined following the Rouquerol consistency criteria as described in the literature.[46–48] The pore size distribution was obtained using the Barrett–Joyner–Halenda (BJH) method with the Kruk–Jaroniec–Sayari correction.[49] The zeta-potential of each mineral was measured using a Malvern Nano ZS Zetasizer with a DTS1070 Folded Capillary Data Cell. All measurements were carried out at target pH levels of 4, 5, 6.3, and 8.3 (adjusted using NaOH or HNO_3) at concentrations of 4.8 g L^{-1} for goethite, kaolinite, and montmorillonite and 238 mg L^{-1} for ferrihydrite in a 10 mmol L^{-1} $NaNO_3$ solution. Mineral suspensions were placed on a rotator overnight at 40 rpm and the final pH was measured prior to zeta-potential analysis.

Batch experiments

Three types of batch experiments were conducted in this study. First, batch kinetics experiments were performed to determine the time required for PFAS sorption to reach equilibrium for each of the 40 PFASs on each of the four minerals. Second, batch isotherm experiments were performed at four pH levels (4, 5, 6.3, and 8.3) to determine the equilibrium sorption distribution coefficient (K_d) of each of the 40 PFASs on each of the four minerals as a function of pH. Third, batch desorption experiments were performed at pH 4 to determine the extent of desorption of each of the 40 PFASs from each of the four minerals. All batch experiments were performed in triplicate using 15 mL polypropylene (PP) centrifuge tubes (Corning) in a 10 mmol L^{-1} $NaNO_3$ matrix at 23 °C. The general procedure for all batch experiments was previously described.[50–53] Briefly, stock solutions of each of the four minerals were prepared in 20 mL amber glass vials at concentrations of 5 g L^{-1} for

ferrihydrite and 500 g L^{-1} for goethite, kaolinite, and montmorillonite, mixed for 30 minutes on a magnetic stirrer, ultrasonicated for 10 minutes, and spiked into a 15 mL PP centrifuge tube containing 10 mL of 10 mmol L^{-1} $NaNO_3$ to achieve the desired concentration. Next, 20 μL of at least one of the PFAS stock solutions (PSSs) was spiked into each reactor tube to generate an initial concentration of 1 μg L^{-1} for each PFAS. Kinetics experiments and isotherm experiments with ferrihydrite were performed with PSS#1, PSS#2, and PSS#3 in separate reactor tubes; isotherm experiments with goethite, montmorillonite, and kaolinite and all desorption experiments were performed with PSS#1 and PSS#2 in one reactor tube and PSS#3 in a separate reactor tube. The spiked reactor tubes were loaded onto a tube revolver (ThermoFisher Scientific), rotated at 40 rpm and destructively sampled at predetermined time points depending on the experiment type. After removal, 8 mL of the experimental solution was transferred from the reactor tubes to a syringe and filtered into a new 15 mL PP centrifuge tube. Then, 8 mL of the filtrate was transferred to a 10 mL glass LC-MS vial (ThermoFisher Scientific) and spiked with 12 μL of the ILIS mixture (250 μg L^{-1}) to yield a target ILIS concentration (375 ng L^{-1}). The samples were stored at 4 °C until analysis. Control samples were prepared following the same procedure without the addition of a mineral. More details of the three types of batch experiments and subsequent data analyses are provided in text in the SI.

Analytical method

Samples from all batch experiments were measured by means of large-volume injection and high-performance liquid chromatography (HPLC) coupled with high-resolution mass spectrometry (HRMS, quadrupole-Orbitrap, ThermoFisher Scientific) using a parallel reaction monitoring (PRM) method optimized for targeted PFAS quantification that was previously described.[50,51] Details on chromatographic conditions, electrospray ionization (ESI) polarity modes, and other mass spectral (MS) acquisition parameters are provided in text in the SI and in Tables S4 and S5.

Results and discussion

Quality control for PFAS data

All experiments were spiked with one or more of the three PFAS stock solutions (PSSs) that contained a total of 40 PFASs. However, the number of PFASs for which we report data for each type of experiment varies depending on our quality control (QC) criteria. Details on the QC criteria for each type of experiment are provided in text in the SI and a summary of the PFASs for which we report data for each type of batch experiment is provided in Table S6. We note that four long-chain PFASs (C > 8) never passed our QC criteria for any experiment (PFTrDA, PFTA, 9:1:2 FTUCA, and FOSA), and some other long-chain PFASs passed our QC criteria only rarely (fewer than 8 times across the 24 experiments) including PFDoA, PFDS, 10:2 FTCA, 10:2 FTS, and *N*-EtFOSAA. These PFASs likely sorb to our experimental materials[54] or partition to the air–water interface[55] resulting in control concentrations outside the QC threshold. Meanwhile, 27 of the 40 PFASs passed our QC criteria all or most of the time (at least 16 times across the 24 experiments) including the C4–C10 PFCAs, the C6–C8 PFSAs, the 6:2, 8:2, 3:3, 5:3, and 7:3 FTCAs, the 5:1:2 and 7:1:2 FTUCAs, the 6:2 and 8:2 FTSs, FBSA, FBSE, and MeFBSE, and all five zwitterions. The overall result is a somewhat fragmented but high-quality dataset and one that can provide insight into the sorption (and desorption) of a variety of PFASs on each of the four minerals.

Mineral characterization

PFAS sorption kinetics and equilibrium sorption of PFASs on the four minerals are expected to be influenced by the particle size of the mineral, the morphology and surface area of the mineral, and the surface charge of the mineral.[43,56] To control differences in PFAS sorption kinetics and equilibrium sorption of PFASs on the four minerals related to particle size, all minerals were crushed and sieved to a particle size range of 10–38 μm. We used gas sorption measurements to measure the BET surface area, pore volume, and pore diameter of each mineral (Table S3). We note that ferrihydrite and montmorillonite have relatively high surface area and pore volume and a relatively low average pore diameter when compared to goethite and kaolinite. To assess the surface charge of each mineral, we measured zeta-potential as a function of pH and compared the measured values to those reported in the literature. Our experimental data are summarized in Table S7 and presented visually in Fig. S1. Our measured point-of-zero-charge (PZC) values were approximately 7.3 for ferrihydrite, 5.8 for goethite, and less than 4 for montmorillonite and kaolinite. These values generally agree with published values in the literature,[20,36,39,57,58] although our measured PZC for goethite is somewhat lower than the typically reported range of 7.5–9.5.[29–31]

Kinetics experiments

The goal of the kinetics experiments was to identify the time required for equilibrium sorption to be complete under the conditions of our experiments. Our criterion to determine when a PFAS reached equilibrium was defined as the time point (t) when the %adsorption at time t was not significantly different than the %adsorption at time $t - 1$ (Student's t-test, $p < 0.05$). We conducted kinetics experiments at 238 mg L^{-1} for ferrihydrite and 23.8 g L^{-1} for goethite, kaolinite, and montmorillonite as detailed in the SI; the 100-fold difference in mineral concentrations is driven by preliminary data that demonstrate greater extents of PFAS sorption on ferrihydrite at lower concentrations. We report data on sorption kinetics for 29 PFASs on ferrihydrite, 27 PFASs on goethite, 31 PFASs on kaolinite, and 32 PFASs on montmorillonite in Table S8 (based on QC requirements and data summarized in Table S6).

We selected equilibrium times of two days for ferrihydrite, four days for goethite, seven days for kaolinite, and seven days for montmorillonite (Table S8). Most PFASs exhibit significantly similar extents of sorption from day 1 to day 2, indicating that sorption equilibrium is reached within 48 hours for many PFASs on all four minerals (23 out of 29 for ferrihydrite, 24 out of 27 for

goethite, 20 out of 31 for kaolinite, and 19 out of 32 for montmorillonite). However, some PFASs exhibit distinct rate-limiting behaviors that result in continued sorption over seven days. This phenomenon was observed for 6:2 FTCA and 6:2 FTS on goethite, 6:2 FTCA, 4:2 FTS, and 8:2 FTS on montmorillonite, and PFUnA and *N*-EtFOSAA on kaolinite (Table S8). It is notable that this phenomenon was not restricted to either iron oxide or silica clay minerals and was primarily observed for polyfluoroalkyl substances. We interpret these data as evidence of multiple sorption mechanisms that exhibit different rate-limiting behaviors.[59,60] Despite the value of these bulk observations on sorption kinetics, we note that the kinetics experiments were not designed with sufficient temporal resolution to enable estimation of rate constants or more mechanistic interpretations of rate-limiting behaviors.

Isotherm experiments

The goal of the isotherm experiments was to determine the equilibrium sorption distribution coefficient (K_d) of each of the 40 PFASs on each of the four minerals as a function of pH. We conducted isotherm experiments at three mineral doses (10, 48, and 238 mg L^{-1} for ferrihydrite and 1.0, 4.8, and 23.8 g L^{-1} for goethite, kaolinite, and montmorillonite as detailed in the SI) to ensure that we were estimating K_d values in the linear range of the otherwise nonlinear isotherm.[52,61] We note that 71.1% of the three-point isotherms exhibited linearity across all three points, while the remaining isotherms deviated from the expected linearity. In these latter cases, the log K_d value was estimated from the fraction of the data within the linear range as detailed in the SI. We report the average equilibrium sorption distribution coefficient (as log K_d values) from the triplicate experiments at each pH value as a function of pH for 34 PFASs on ferrihydrite, 32 PFASs on goethite, 32 PFASs on montmorillonite, and 31 PFASs on kaolinite in Tables S9 through S12, respectively. We note that the pH levels were fixed at the beginning of each experiment and were adjusted periodically throughout the equilibration period to maintain the target pH.

Overall dataset. Box plots displaying the range of log K_d values for each PFAS at all pH levels on each of the four minerals are provided as Fig. 2. The data demonstrate that PFASs exhibit higher log K_d values on ferrihydrite *versus* goethite among the iron oxide minerals and higher log K_d values on montmorillonite *versus* kaolinite among the silica clay minerals. This distribution may be linked to the relative surface area and pore volume of each of the mineral types, with ferrihydrite and montmorillonite exhibiting relatively higher values (Table S3). The distributions of log K_d values among all four minerals are also significantly different from each other, with the most similar distributions found between goethite and montmorillonite (Student's *t*-test, $p = 0.02$). The data also demonstrate that the average log K_d values among the PFASs range over at least three orders of magnitude for each of the four minerals, reflecting important differences in the potential of different PFASs to sorb to each of the four minerals.

Comparison among the minerals. Due to the similarities in surface chemistry, we reasoned that the dominant sorption mechanisms on the two iron oxide minerals and the two silica clay minerals should be similar and that differences in the magnitudes of the log K_d values reflect the relative affinity of the dominant sorption mechanisms for each PFAS on the different minerals. If this expectation holds true, then we would expect that plotting the log K_d values of the iron oxide and silica clay minerals against each other would produce a monotonic relationship that favors ferrihydrite and montmorillonite (based on data in Fig. 2) and that any outliers from this relationship reflect PFASs that participate in sorption mechanisms that are stronger than one would predict from the monotonic relationship on one of the minerals.

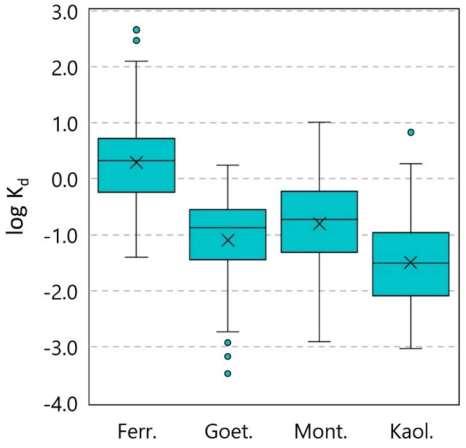

Fig. 2 Box plot of all average log K_d values (units are L g^{-1} prior to log transformation) measured across all pH levels for ferrihydrite ($n = 124$), goethite ($n = 106$), kaolinite ($n = 111$), and montmorillonite ($n = 117$). The box represents the interquartile range of values, the horizontal line inside the box represents the median, the *X* inside the box represents the mean, and the whiskers represent the range of the data outside the interquartile range. Outliers for ferrihydrite are for *N*-MeFOSAA (2.66 @ pH 5) and *N*-EtFOSAA (2.47 @ pH 5). Outliers for goethite are for AmPr-FHxSA (−3.48 @ pH 8.3), 10:2 FTS (−3.18 @ pH 5 and −3.09 @ pH 6.3), and FBSE (−3.09 @ pH 8.3). Outliers for kaolinite are 10:2 FTCA (0.85 @ pH 5) and 6:2 FTCA (0.83 @ pH 5).

In Fig. 3a, we plot the log K_d values of goethite *versus* ferrihydrite along with the overall trend line and the ±0.5 log unit offsets. The trend line exhibits the expected significant positive slope and intercept and 68% of the observations fall within the ±0.5 log unit offsets demonstrating that the trend in the magnitudes of the average log K_d values between the two iron oxide minerals is monotonic and linear (Pearson's $R = 0.5721$, $p < 0.00001$). The log K_d values that fall below the −0.5 log unit offset represent PFASs that exhibit stronger affinity for ferrihydrite than one would predict from the linear relationship relative to the affinity for goethite at a particular pH value. Twenty percent of the data fall in this category and represent the log K_d values of PFBA and PFPeA at all pH values; PFHxA, PFHpA, and PFOA at a pH of 8.3 (these are the C4–C8 PFCAs, blue diamonds), PFHxS and PFHpS at a pH of 8.3 (C7–C8 PFSAs, blue triangles), 4:2 FTS (red circle) and FBSA (red diamond) at all pH values, and 7:3 FTCA (blue square) at a pH of 8.3 among a few other sporadic observations. These data demonstrate that ferrihydrite has higher affinity than what would be predicted for

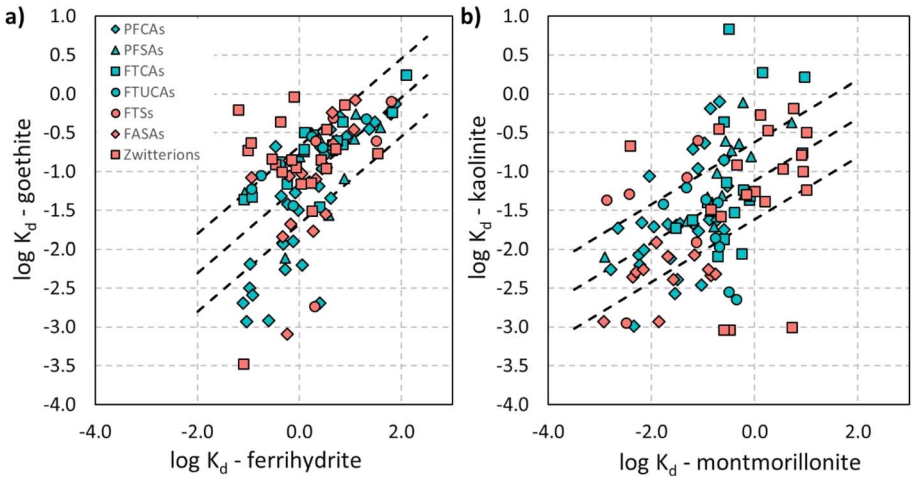

Fig. 3 Comparison of average log K_d values (units are L g^{-1} prior to log transformation) among the (a) iron oxide minerals (ferrihydrite and goethite) and (b) silica clay minerals (montmorillonite and kaolinite). The center dashed line represents the trend line through all of the data, and the upper and lower lines represent ±0.5 log unit of deviation from the trend line.

short-chain PFASs (C4–C5) at all pH values and mid-chain PFASs (C6–C8) at a pH of 8.3. The former observation could be linked to the greater pore volume and higher surface area of ferrihydrite which may enable relatively short-chain PFASs to diffuse into the mineral particle and access sites that are inaccessible to mid- or long-chain PFASs, in addition to providing greater numbers of sorption sites that may also limit sorption competition.[60,62] The latter observation suggests that the phenomenon extends to include mid-chain PFASs at a pH of 8.3 when goethite (PZC = 5.8) has a more strong net negative surface charge than ferrihydrite (PZC = 7.3). Conversely, the log K_d values that fall above the +0.5 log unit offset represent PFASs that exhibit stronger affinity for goethite than one would predict from the linear relationship and twelve percent of the data fall in this category. The PFASs in this category include the zwitterionic PFASs 5:3 FTB and 5:1:2 FTB at pH 6.3 or 8.3 and AmPr-FHxSA and TAmPr-FHxSA at pH 4 and 5 (red squares). At pH values of 6.3 and 8.3, goethite is expected to have a more strong net negative surface charge than ferrihydrite, which may promote favorable electrostatic interactions with the internal quaternary ammonium (cationic functional group) on 5:3 FTB and 5:1:2 FTB.[63] At pH values of 4 and 5, goethite is expected to have a weaker net positive surface charge than ferrihydrite, which may enable relatively weak yet favorable electrostatic interactions with the terminal amine (cationic functional group) on AmPr-FHxSA and TAmPr-FHxSA and residual negatively charged surface sites.[63]

In Fig. 3b, we plot the log K_d values of kaolinite *versus* montmorillonite along with the overall trend line and the ±0.5 log unit offsets. The trend line exhibits the expected significant positive slope and intercept, and 57% of the observations fall within the ±0.5 log unit offsets (Pearson's $R = 0.4789$, $p < 0.00001$). Despite meeting our expectation, the data for the silica clay minerals are more scattered and exhibit fewer clear relationships than what we observed for the iron oxide minerals. This is likely due to the more pronounced differences in the morphology of montmorillonite *versus* kaolinite when compared to the iron oxide minerals. Nevertheless, one clear trend is higher average log K_d values than one would predict from the linear relationship for relatively short-chain PFASs at all pH levels for montmorillonite. This includes data for PFBA, PFHxA, PFHpA, 3:3 FTCA, 5:3 FTCA, FBSA, FBSE, and MeFBSE. This observation could again be linked to the greater pore volume and higher surface area of montmorillonite which enables relatively short-chain PFASs to diffuse into the mineral particle and access sites that are inaccessible to mid- or long-chain PFASs, in addition to providing greater numbers of sorption sites that may also limit sorption competition.[60,62] Another trend is the stronger sorption than one would predict from the linear relationship of mid- and long-chain PFCAs (PFOA, PFNA, and PFDA), PFSAs (PFHpS and PFOS), FTCAs, (6:2 FTCA and 8:2 FTCA), and the FTSs at varying pH levels on kaolinite. This could be explained by the more hydrophobic character of kaolinite, which is favorable for sorption of mid- and long-chain PFASs.[38,43] A final trend worth mentioning is the stronger sorption of AmPr-FHxSA and TAmPr-FHxSA than one would predict from this linear relationship on kaolinite at all pH levels. This could be linked to the potential of the internal anionic sulfonamide group to interact favorably with the positively charged edge sites of kaolinite, although more mechanistic studies would need to be conducted to provide insights into the specific mechanism.[63]

Comparison among the PFASs – effect of pH levels. The PFASs selected for this study exhibit a wide range of pK_a values (Table S4). All the PFCAs, PFSAs, FTUCAs, FTSs, and *N*-MeFOSAA and *N*-EtFOSAA have pK_a values that are lower than 3, which indicates that these PFASs will all be primarily anionic at all of the pH levels studied. However, the FTCAs have pK_a values that range between 2.6 and 4.2, indicating that some fraction of the FTCAs will be neutral at pH 4. Likewise, the FASAs have pK_a values in the range of 6.1–8.1, which indicates that they will likely be mostly neutral at pH 4, 5, and 6.3, but more anionic at

pH 8.3. Finally, the zwitterions have two ionizable functional groups that might be protonated or deprotonated within the pH range of the experiments. We expect 5:3 FTB, 5:1:2 FTB, and 6:2 FTAB to be zwitterionic at all pH levels and AmPr-FHxSA and TAmPr-FHxSA to be at least partially cationic at pH 4 and 5. As such, we can classify the seven classes of PFASs included in this study as those that are always anionic (PFCAs, PFSAs, FTUCAs, and FTSs), those that are neutral at low pH and anionic at high pH (FTCAs and FASAs), and those that are zwitterionic or cationic at low pH (zwitterions). We present log K_d values as a function of pH for eight representative PFASs including four always anionic PFASs, two neutral or anionic PFASs, and two zwitterionic PFASs on all four minerals in Fig. 4.

Fig. 4a and b demonstrate the pH-dependency of the log K_d values for eight representative PFASs on ferrihydrite and goethite. The data reveal the clear negative association between log K_d values and pH for the four representative always anionic PFASs and the two representative neutral and anionic PFASs on these iron oxide minerals. It is interesting to note that the average log K_d values for PFHpS increase from a pH level of 6.3 to a pH level of 8.3 on ferrihydrite. This is an unexpected behavior, but one that is consistent and repeatable for PFHpS across all of our experiments with ferrihydrite and is also observed for several other always anionic PFASs in the dataset (Table S9). The zwitterionic PFASs exhibit distinct behavior on the two iron oxide minerals that highlights the relative roles of their two ionizable functional groups. The log K_d values of 5:3

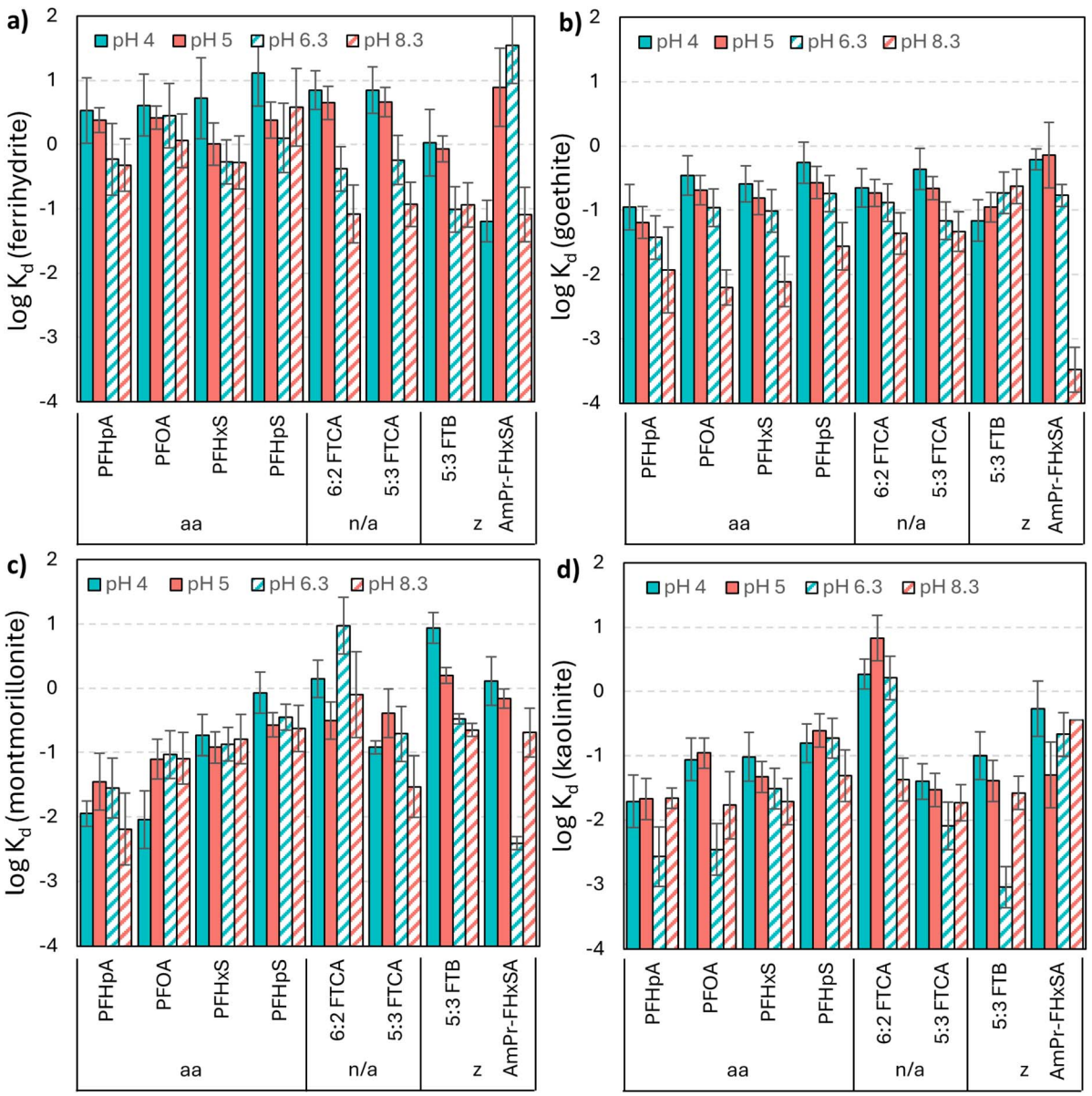

Fig. 4 Comparison of average log K_d values (units are L g^{-1} prior to log transformation) for 8 PFASs as a function of pH for (a) ferrihydrite, (b) goethite, (c) montmorillonite, and (d) kaolinite. aa = PFASs that are always anionic. n/a = PFASs that are neutral at low pH and anionic at high pH. z = zwitterions. Error bars represent standard deviation of triplicate experiments.

FTB decrease with increasing pH on ferrihydrite and increase with increasing pH on goethite. These trends suggest that the terminal carboxylic acid (anionic functional group) may play a role in the sorption of 5:3 FTB on ferrihydrite whereas the internal quaternary ammonium (cationic functional group) may play a role in the sorption of 5:3 FTB on goethite. The $\log K_d$ values of AmPr-FHxSA exhibit relatively low values at pH 4 and 8.3 on ferrihydrite. This trend suggests electrostatic repulsion of the cationic AmPr-FHxSA at pH 4 and electrostatic repulsion driven by the anionic internal sulfonamide nitrogen at pH 8.3. In contrast, $\log K_d$ values of AmPr-FHxSA exhibit relatively low values only at 8.3 on goethite. This suggests that residual negatively charged surface sites on goethite (PZC = 5.8) may enable favorable electrostatic interactions with the cationic terminal amine on AmPr-FHxSA.

Fig. 4c and d demonstrate the weaker pH-dependency of the $\log K_d$ values for eight representative PFASs on montmorillonite and kaolinite. The data reveal that there is no significant trend between the $\log K_d$ values and pH for the four representative always anionic PFASs and the two representative neutral and anionic PFASs on montmorillonite and kaolinite (Student's *t*-test, $p > 0.05$). There is likewise no significant trend between the $\log K_d$ values and pH for the two representative zwitterions (Student's *t*-test, $p > 0.05$). One exception is the clearly decreasing $\log K_d$ values for 5:3 FTB and 5:1:2 FTB (Table S11) with increasing pH on montmorillonite. This is an unexpected trend that demonstrates that the increasing speciation of the terminal carboxylic acid (anionic functional group) must exhibit unfavorable interactions with the increasing negative surface charge of montmorillonite.

Although the detailed evaluation of $\log K_d$ values as a function of pH for representative PFASs is important (Fig. 4), our relatively large dataset presented in Tables S9 and S12 provides opportunities to examine significant associations more broadly across the seven PFAS classes. For example, we identified significant negative associations between the average $\log K_d$ values for six of the PFAS classes (all except the zwitterionic PFASs) and the pH level of the experiment for both of the iron oxide minerals. The significance of this association is greater for those PFASs that are neutral at low pH and anionic at high pH (Student's *t*-test, $p = 0.0005$ for ferrihydrite; $p = 0.004$ for goethite) than for those PFASs that are always anionic (Student's *t*-test, $p = 0.001$ for ferrihydrite; $p = 0.02$ for goethite). These observations demonstrate the importance of the surface charge of the mineral (PZC for ferrihydrite = 7.3; PZC for goethite = 5.8) and the speciation of the PFAS on sorption. At higher pH levels, both the sorbent and the sorbate are more likely to be anionic and the average $\log K_d$ values decrease due to electrostatic repulsion.[20,26,28,42] We identified no significant relationship between the average $\log K_d$ values for any of the seven classes of PFASs and the pH level of the experiment for the silica clay minerals. In this case, the lack of a pH dependence is more likely linked to the consistently negative surface charge of the silica clay minerals over all of the studied pH levels. Together, our data indicate that changes in the surface charge of the mineral are important for the sorption of some PFASs on iron oxide mineral surfaces and that changes in the speciation of the PFASs can amplify this effect.

Comparison among the PFASs – effect of perfluoroalkyl chain length. We have already discussed the higher average $\log K_d$ values for relatively short-chain PFASs for the minerals with higher pore volumes and surface area. We now aim to explore the effect of perfluoroalkyl chain length on average $\log K_d$ values more comprehensively across the PFASs. Increases in the perfluoroalkyl chain length of a PFAS can influence sorption in several ways including increasing the hydrophobicity of the PFAS and increasing the density of electrons in the perfluoroalkyl chain resulting in a stronger partial negative charge.[14,20] To explore the effect of perfluoroalkyl chain length on the sorption of PFASs on each mineral, we present the relationship between average $\log K_d$ values and the number of fluorinated carbon atoms in each PFAS in Fig. 5. We do not include zwitterions in this analysis because they all have five or six fluorinated carbon atoms, yielding insufficient data to observe a relationship with perfluoroalkyl chain length.

The data demonstrate positive and significant associations between the average $\log K_d$ values for all PFASs and their respective perfluoroalkyl chain length for all four minerals (Student's *t*-test, $p < 0.00001$ for all minerals). Hydrophobic interactions are unlikely to explain the higher sorption of long-chain PFASs compared to short-chain PFASs on the hydrophilic iron oxides.[13,14,20,56,64] Therefore, we hypothesize that this phenomenon is linked to the weak negative charge of each additional fluorine atom which induces H-bonding between the partially positively charged surface functional groups on the iron oxide minerals.[14,20] In contrast, hydrophobic interactions may play an important role in the sorption of PFASs on the silica clays.[15,45,65] This could be due to hydrophobic interactions between PFASs and hydrophobic patches on the siloxane surface of the clay minerals.[38] The hydrophobic patch surface area of montmorillonite as a means for PFAS sorption may be relatively limited and as a result the sorption of long-chain PFASs may likewise be limited.[66]

Desorption experiments

The goal of the desorption experiments was to determine the reversibility of PFAS sorption on each of the four minerals. We performed all desorption experiments at a pH of 4 because most PFASs exhibited the highest $\log K_d$ values for each of the four minerals at this pH value and we reasoned that desorption would be best quantified after the greatest extent of sorption. We performed desorption experiments at 48 mg L^{-1} for ferrihydrite and 4.8 g L^{-1} for goethite, kaolinite, and montmorillonite over three desorption cycles as detailed in the SI and calculated the percent desorption of each PFAS after each desorption cycle using eqn (S7) and eqn (S8). Following application of stringent QC criteria and the added criterion that some significant fraction of PFASs had to be sorbed to observe desorption, we report the percent desorption for 11 PFASs for ferrihydrite, 7 PFASs for goethite, 7 PFASs for montmorillonite, and 5 PFASs for kaolinite in Fig. 6.

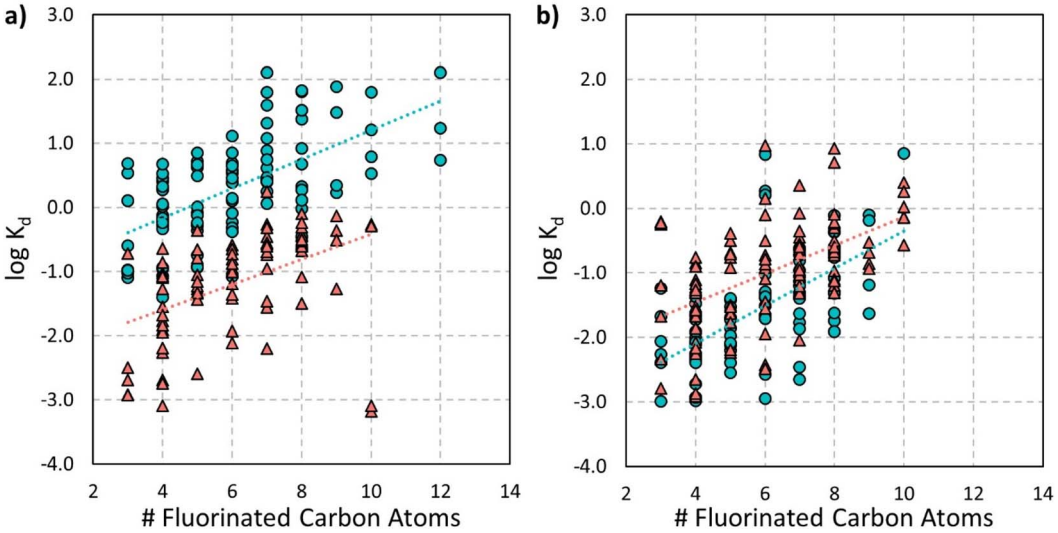

Fig. 5 Relationship between average log K_d values (units are L g^{-1} prior to log transformation) and the number of fluorinated carbon atoms in each PFAS for (a) the iron oxide minerals ferrihydrite (blue circles) and goethite (red triangles) and (b) silica clay minerals kaolinite (blue circles) and montmorillonite (red triangles). Zwitterions are not included in this plot because they all have five or six fluorinated carbon atoms, yielding insufficient data to observe a relationship.

Despite the limited data available to evaluate desorption, our data reveal several important phenomena. First, all PFASs for which percent desorption could be calculated exhibited nearly complete desorption after only two desorption cycles. We attribute the incomplete recovery of some PFASs on some minerals to analytical uncertainties because no additional desorption was observed for those PFASs in subsequent desorption cycles. Complete desorption after one or two desorption cycles is unexpected as we anticipated desorption that adheres to our log K_d values with perhaps some extent of sorption hysteresis. Nevertheless, this observation demonstrates that the sorption in our experiments is reversible, which indicates that sorption on these minerals would only retard the transport of PFASs in groundwater as opposed to fully capture and sequester them. This is important in the context of bioavailability and biotransformation; it is possible that some PFASs that are sorbed to aquifer minerals will have limited bioavailability, but those PFASs that desorb will be susceptible to biotransformation and are likely to be biotransformed into more mobile PFAAs.[19] In other words, as PFASs in the aqueous phase are transformed, surface-bound compounds will then readily desorb to maintain a dynamic equilibrium, so even compounds with relatively high log K_d values can be subject to biotransformation. Second, desorption from iron oxide minerals is more facile than desorption from silica clay minerals. For example, 5:1:2 FTUCA exhibits nearly complete

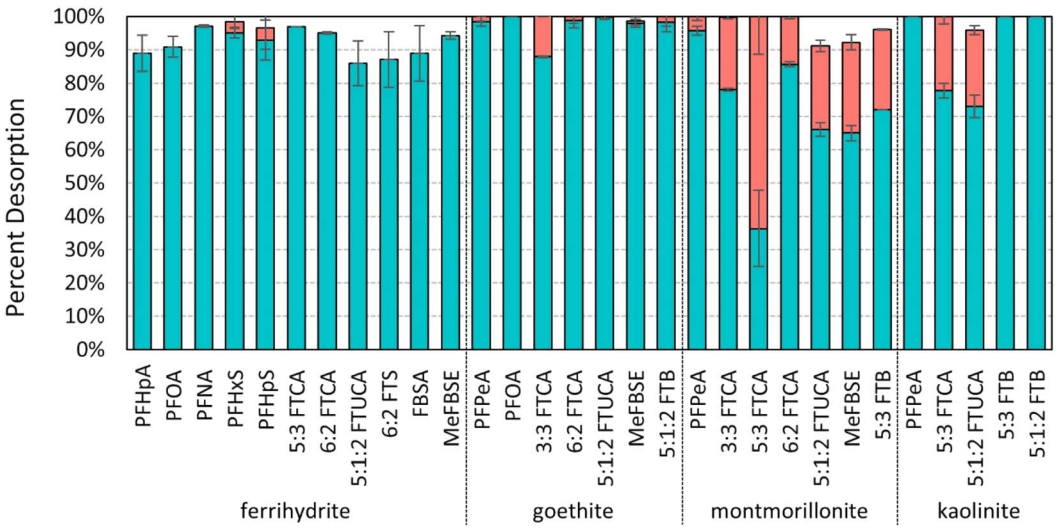

Fig. 6 Percent desorption of all PFASs that met our stringent QC criteria on each of the four minerals after one desorption cycle (blue) and two desorption cycles (red).

desorption from the iron oxide minerals after one desorption cycle, whereas only 66% and 73% of 5:1:2 FTUCA is desorbed after the first desorption cycle for montmorillonite and kaolinite, respectively. This observation supports the hypothesis that PFAS sorption on the iron oxide minerals is driven by relatively weak electrostatic interactions and H-bonding.[15] In contrast, PFAS sorption on the silica clay minerals may be driven by more hydrophobic interactions and relatively strong and less reversible types of electrostatic interactions.[59,67] Third, we observe less desorption for FTCAs, FTUCAs, and FASAs after the first desorption cycle on the silica clay minerals. We attribute this observation to the potential for these classes of PFASs to act as both an H-donor and H-acceptor at pH 4, enhancing their potential to interact with clay edge sites.[56,64] Finally, some PFASs exhibit complete desorption from kaolinite after one desorption cycle, but there is incomplete desorption across all PFASs after one desorption cycle for montmorillonite. One explanation lies in the interlayer spaces of montmorillonite that can accommodate PFAS intercalation, suggesting a mechanism of entrapment for sorption on montmorillonite.[16,68]

Conclusions

To the best of our knowledge, this study provides the most comprehensive set of $\log K_d$ values for a diverse set of PFASs on ubiquitous and highly abundant aquifer materials. To generate such a comprehensive dataset, we performed all of our experiments with mixtures of diverse sets of PFASs. Although this was essential to meet our objectives, we acknowledge that sorption competition among the PFASs was not explicitly addressed. Nevertheless, the data provided in Tables S9 through S12 can be used in fate and transport models to simulate the transport of diverse types of PFASs from source zones and other impacted environments where they will likewise be present in mixtures. These data will be of great value to remediation project managers, hydrogeologists, and environmental engineers who need to make important decisions on how to address impacted sites based on the best available data. In particular, the inclusion of less studied PFASs in this study (*e.g.*, FTCAs, FTUCAs, FASAs, and zwitterions) not only provides previously unreported $\log K_d$ values for these classes of PFASs, but also provides new insights on the potential mechanisms driving their sorption and desorption from aquifer materials. Our relatively large dataset can also be used to support future studies that rely on machine learning to make predictions of $\log K_d$ values of unstudied PFASs or to simulate the sorption of the selected PFASs on unstudied aquifer materials. Together, our data make practical contributions to support site characterization and remediation efforts, while also contributing key insights into the fundamental sorption processes.

Conflicts of interest

There are no conflicts to declare.

Data availability

The data supporting this article have been included as part of the supplementary information (SI). Supplementary information: text providing additional details on the three types of batch experiments, the analytical methods, and the quality control measures applied for PFAS data; zeta-potential measurements for each mineral at varying pH levels (Fig. S1 and Table S7); details on PFAS standards, isotope-labelled internal standards, and all other chemicals and reagents (Tables S1 and S2); details on the properties of the four minerals (Table S3); analytical details (Tables S4 and S5); summary of quality control criteria (Table S6); summary of adsorption kinetics (Table S8); and all solids-water partitioning coefficients for each PFAS and each mineral at each pH level (Tables S9–S12). See DOI: https://doi.org/10.1039/d5em00847f.

Acknowledgements

This work was supported by the Strategic Environmental Restoration and Development Program (SERDP) under project identifier ER23-3697. Gas sorption measurements were supported by the National Science Foundation (CBET-2047627) (D. K. and P. J. M.). Any opinions, findings, and conclusions or recommendations expressed in this material are those of the author(s) and do not necessarily reflect the views of the National Science Foundation. We also acknowledge support from a Camille Dreyfus Teacher-Scholar Award to P. J. M. (TC-23-048).

References

1 I. T. Cousins, J. C. DeWitt, J. Glüge, G. Goldenman, D. Herzke, R. Lohmann, M. Miller, C. A. Ng, M. Scheringer, L. Vierke and Z. Wang, Strategies for grouping per- and polyfluoroalkyl substances (PFAS) to protect human and environmental health, *Environ. Sci.: Processes Impacts*, 2020, **22**, 1444–1460.

2 E. M. Sunderland, X. C. Hu, C. Dassuncao, A. K. Tokranov, C. C. Wagner and J. G. Allen, A Review of the Pathways of Human Exposure to Poly- and Perfluoroalkyl Substances (PFASs) and Present Understanding of Health Effects, *J. Exposure Sci. Environ. Epidemiol.*, 2019, **29**, 131–147.

3 A. Nickerson, A. C. Maizel, P. R. Kulkarni, D. T. Adamson, J. J. Kornuc and C. P. Higgins, Enhanced Extraction of AFFF-Associated PFASs from Source Zone Soils, *Environ. Sci. Technol.*, 2020, **54**, 4952–4962.

4 A. Nickerson, A. E. Rodowa, D. T. Adamson, J. A. Field, P. R. Kulkarni, J. J. Kornuc and C. P. Higgins, Spatial Trends of Anionic, Zwitterionic, and Cationic PFASs at an AFFF-Impacted Site, *Environ. Sci. Technol.*, 2021, **55**, 313–323.

5 D. T. Adamson, A. Nickerson, P. R. Kulkarni, C. P. Higgins, J. Popovic, J. Field, A. Rodowa, C. Newell, P. DeBlanc and J. J. Kornuc, Mass-Based, Field-Scale Demonstration of PFAS Retention within AFFF-Associated Source Areas, *Environ. Sci. Technol.*, 2020, **54**, 15768–15777.

6 N. T. Joseph, T. Schwichtenberg, D. Cao, G. D. Jones, A. E. Rodowa, M. A. Barlaz, J. A. Charbonnet, C. P. Higgins,

J. A. Field and D. E. Helbling, Target and Suspect Screening Integrated with Machine Learning to Discover Per- and Polyfluoroalkyl Substance Source Fingerprints, *Environ. Sci. Technol.*, 2023, **57**, 14351–14362.

7 E. Hepburn, C. Madden, D. Szabo, T. L. Coggan, B. Clarke and M. Currell, Contamination of groundwater with per- and polyfluoroalkyl substances (PFAS) from legacy landfills in an urban re-development precinct, *Environ. Pollut.*, 2019, **248**, 101–113.

8 S. Felizeter, H. Jürling, M. Kotthoff, P. De Voogt and M. S. McLachlan, Influence of soil on the uptake of perfluoroalkyl acids by lettuce: A comparison between a hydroponic study and a field study, *Chemosphere*, 2020, **260**, 127608.

9 Y. Katsenovich, B. Tansel, N. Soares Quinete, Z. Nasir, J. O. Ocheje and M. M. Manzano, Leaching profile of per- and polyfluoroalkyl substances (PFAS) from biosolids after thickening, anaerobic digestion, and dewatering processes, and significance of protein, phosphorus, and selected ions, *Sci. Total Environ.*, 2024, **957**, 177777.

10 T. Schroeder, D. Bond and J. Foley, PFAS soil and groundwater contamination: Via industrial airborne emission and land deposition in SW Vermont and Eastern New York State, USA, *Environ. Sci.: Processes Impacts*, 2021, **23**, 291–301.

11 C. A. Moody, G. N. Hebert, S. H. Strauss and J. A. Field, Occurrence and persistence of perfluorooctanesulfonate and other perfluorinated surfactants in groundwater at a fire-training area at Wurtsmith Air Force Base, Michigan, USA, *J. Environ. Monit.*, 2003, **5**, 341–345.

12 M. Murakami, K. Kuroda, N. Sato, T. Fukushi, S. Takizawa and H. Takada, Groundwater Pollution by Perfluorinated Surfactants in Tokyo, *Environ. Sci. Technol.*, 2009, **43**, 3480–3486.

13 Y. Zhao, X. Min, S. Xu and Y. Wang, Adsorption of Per- and Polyfluoroalkyl Substances (PFAS) by Aquifer Materials: the Important Role of Dolomite, *Environ. Sci. Technol.*, 2023, **10**, 931–936.

14 C. P. Higgins and R. G. Luthy, Sorption of perfluorinated surfactants on sediments, *Environ. Sci. Technol.*, 2006, **40**, 7251–7256.

15 R. S. Kookana, D. A. Navarro, S. Kabiri and M. J. McLaughlin, Key properties governing sorption–desorption behaviour of poly- and perfluoroalkyl substances in saturated and unsaturated soils: a review, *Soil Res.*, 2022, **61**, 107–125.

16 F. Xiao, B. Jin, S. A. Golovko, M. Y. Golovko and B. Xing, Sorption and Desorption Mechanisms of Cationic and Zwitterionic Per- and Polyfluoroalkyl Substances in Natural Soils: Thermodynamics and Hysteresis, *Environ. Sci. Technol.*, 2019, **53**, 11818–11827.

17 D. T. Adamson, P. R. Kulkarni, A. Nickerson, C. Higgins, J. A. Field, T. Schwichtenberg, C. Newell and J. J. Kornuc, Characterization of relevant site specific PFAS fate and transport processes at multiple AFFF sites, *Environ. Adv.*, 2022, **7**, 100167.

18 M. W. Sima and P. R. Jaffé, A critical review of modeling Poly- and Perfluoroalkyl Substances (PFAS) in the soil-water environment, *Sci. Total Environ.*, 2021, **757**, 143793.

19 F. Geng and D. E. Helbling, Cascading Pathways Regulate the Biotransformations of Eight Fluorotelomer Acids Performed by Wastewater Microbial Communities, *Environ. Sci. Technol.*, 2024, **58**, 23201–23211.

20 H. Campos-Pereira, D. B. Kleja, C. Sjöstedt, L. Ahrens, W. Klysubun and J. P. Gustafsson, The Adsorption of Per- and Polyfluoroalkyl Substances (PFASs) onto Ferrihydrite Is Governed by Surface Charge, *Environ. Sci. Technol.*, 2020, **54**, 15722–15730.

21 T. M. H. Nguyen, J. Bräunig, R. S. Kookana, S. L. Kaserzon, E. R. Knight, H. N. P. Vo, S. Kabiri, D. A. Navarro, C. Grimison, N. Riddell, C. P. Higgins, M. J. McLaughlin and J. F. Mueller, Assessment of Mobilization Potential of Per- and Polyfluoroalkyl Substances for Soil Remediation, *Environ. Sci. Technol.*, 2022, **56**, 10030–10041.

22 F. Xiao, X. Zhang, L. Penn, J. S. Gulliver and M. F. Simcik, Effects of Monovalent Cations on the Competitive Adsorption of Perfluoroalkyl Acids by Kaolinite: Experimental Studies and Modeling, *Environ. Sci. Technol.*, 2011, **45**, 10028–10035.

23 Yu. V. Knyazev, D. A. Balaev, S. V Stolyar, O. A. Bayukov, R. N. Yaroslavtsev, V. P. Ladygina, D. A. Velikanov and R. S. Iskhakov, Magnetic anisotropy and core-shell structure origin of the biogenic ferrihydrite nanoparticles, *J. Alloys Compd.*, 2021, **851**, 156753.

24 S. J. Smith, K. Page, H. Kim, B. J. Campbell, J. Boerio-Goates and B. F. Woodfield, Novel Synthesis and Structural Analysis of Ferrihydrite, *Inorg. Chem.*, 2012, **51**, 6421–6424.

25 T. Hiemstra and W. H. Van Riemsdijk, A surface structural model for ferrihydrite I: Sites related to primary charge, molar mass, and mass density, *Geochim. Cosmochim. Acta*, 2009, **73**, 4423–4436.

26 J. A. Davis and J. O. Leckie, Surface ionization and complexation at the oxide/water interface II. Surface properties of amorphous iron oxyhydroxide and adsorption of met al ions, *J. Colloid Interface Sci.*, 1978, **67**, 90–107.

27 L. Notini, L. K. ThomasArrigo, R. Kaegi and R. Kretzschmar, Coexisting Goethite Promotes Fe(II)-Catalyzed Transformation of Ferrihydrite to Goethite, *Environ. Sci. Technol.*, 2022, **56**, 12723–12733.

28 R. L. Johnson, A. J. Anschutz, J. M. Smolen, M. F. Simcik and R. Lee Penn, The adsorption of perfluorooctane sulfonate onto sand, clay, and iron oxide surfaces, *J. Chem. Eng. Data*, 2007, **52**, 1165–1170.

29 M. Kosmulski, E. Maczka, E. Jartych and J. B. Rosenholm, Synthesis and characterization of goethite and goethite–hematite composite: experimental study and literature survey, *Adv. Colloid Interface Sci.*, 2003, **103**, 57–76.

30 C. Y. Tang, Q. Shiang Fu, D. Gao, C. S. Criddle and J. O. Leckie, Effect of solution chemistry on the adsorption of perfluorooctane sulfonate onto mineral surfaces, *Water Res.*, 2010, **44**, 2654–2662.

31 J. Uwayezu, L. Yeung and M. Bäckström, Sorption of PFOS isomers on goethite as a function of pH, dissolved or ganic

matter (humic and fulvic acid) and sulfate, *Chemosphere*, 2019, **233**, 896–904.
32 R. H. Vora and K. S. Y. Lau, in *Handbook of Thermoset Plastics*, ed. H. Dodiuk, William Andrew Publishing, Boston, 4th edn, 2022, pp. 517–585.
33 C. Zhou, D. Tong and W. Yu, in *Nanomaterials from Clay Minerals*, ed. A. Wang and W. Wang, Elsevier, 2019, pp. 335–364.
34 J. A. R. Willemsen, S. C. B. Myneni and I. C. Bourg, Molecular Dynamics Simulations of the Adsorption of Phthalate Esters on Smectite Clay Surfaces, *J. Phys. Chem. C*, 2019, **123**, 13624–13636.
35 K. W. Weissmahr, S. B. Haderlein and R. P. Schwarzenbach, Complex Formation of Soil Minerals with Nitroaromatic Explosives and other π-Acceptors, *Soil Sci. Soc. Am. J.*, 1998, **62**, 369–378.
36 C. O. Ijagbemi, M.-H. Baek and D.-S. Kim, Montmorillonite surface properties and sorption characteristics for heavy metal removal from aqueous solutions, *J. Hazard. Mater.*, 2009, **166**, 538–546.
37 N. Kumar, M. P. Andersson, D. Van Den Ende, F. Mugele and I. Siretanu, Probing the Surface Charge on the Basal Planes of Kaolinite Particles with High-Resolution Atomic Force Microscopy, *Langmuir*, 2017, **33**, 14226–14237.
38 N. Loganathan and A. K. Wilson, Adsorption, Structure, and Dynamics of Short- and Long-Chain PFAS Molecules in Kaolinite: Molecular-Level Insights, *Environ. Sci. Technol.*, 2022, **56**, 8043–8052.
39 E. Tombácz and M. Szekeres, Surface charge heterogeneity of kaolinite in aqueous suspension in comparison with montmorillonite, *Appl. Clay Sci.*, 2006, **34**, 105–124.
40 J. Cogorno and M. Rolle, Impact of Variable Water Chemistry on PFOS-Goethite Interactions: Experimental Evidence and Surface Complexation Modeling, *Environ. Sci. Technol.*, 2024, **58**, 1731–1740.
41 A. Chaudhary, M. Usman, W. Cheng, S. Haderlein, J.-F. Boily and K. Hanna, Heavy-Metal Ions Control on PFAS Adsorption on Goethite in Aquatic Systems, *Environ. Sci. Technol.*, 2024, **58**, 20235–20244.
42 X. Gao and J. Chorover, Adsorption of perfluorooctanoic acid and perfluorooctanesulfonic acid to iron oxide surfaces as studied by flow-through ATR-FTIR spectroscopy, *Environ. Chem.*, 2012, **9**, 148.
43 L. Zhao, J. Bian, Y. Zhang, L. Zhu and Z. Liu, Comparison of the sorption behaviors and mechanisms of perfluorosulfonates and perfluorocarboxylic acids on three kinds of clay minerals, *Chemosphere*, 2014, **114**, 51–58.
44 N. Loganathan, L. Ashby, C. E. Schumm and A. K. Wilson, Interfacial adsorption and dynamics of fluorotelomers with soil minerals – mechanistic insights, *Environ. Sci. Nano*, 2025, **12**, 850–862.
45 J. A. R. Willemsen and I. C. Bourg, Molecular dynamics simulation of the adsorption of per- and polyfluoroalkyl substances (PFASs) on smectite clay, *J. Colloid Interface Sci.*, 2021, **585**, 337–346.
46 K. S. Walton and R. Q. Snurr, Applicability of the BET Method for Determining Surface Areas of Microporous Metal−Organic Frameworks, *J. Am. Chem. Soc.*, 2007, **129**, 8552–8556.
47 T. Islamoglu, K. B. Idrees, F. A. Son, Z. Chen, S.-J. Lee, P. Li and O. K. Farha, Are you using the right probe molecules for assessing the textural properties of metal–organic frameworks?, *J. Mater. Chem. A*, 2022, **10**, 157–173.
48 D. A. Gómez-Gualdrón, P. Z. Moghadam, J. T. Hupp, O. K. Farha and R. Q. Snurr, Application of Consistency Criteria To Calculate BET Areas of Micro- And Mesoporous Metal–Organic Frameworks, *J. Am. Chem. Soc.*, 2016, **138**, 215–224.
49 D. W. Kim, D. W. Kang, M. Kang, D. S. Choi, H. Yun, S. Y. Kim, S. M. Lee, J.-H. Lee and C. S. Hong, High Gravimetric and Volumetric Ammonia Capacities in Robust Metal–Organic Frameworks Prepared via Double Postsynthetic Modification, *J. Am. Chem. Soc.*, 2022, **144**, 9672–9683.
50 J. Wang, Z.-W. Lin, W. R. Dichtel and D. E. Helbling, Perfluoroalkyl acid adsorption by styrenic β-cyclodextrin polymers, an ion-exchange resins, and activated carbon is inhibited by matrix const ituents in different ways, *Water Res.*, 2024, **260**, 121897.
51 R. Wang, Z. W. Lin, M. J. Klemes, M. Ateia, B. Trang, J. Wang, C. Ching, D. E. Helbling and W. R. Dichtel, A Tunable Porous β-Cyclodextrin Polymer Platform to Understand and Improve Anionic PFAS Removal, *ACS Cent. Sci.*, 2022, **8**, 663–669.
52 C. Ching, M. J. Klemes, B. Trang, W. R. Dichtel and D. E. Helbling, β-Cyclodextrin Polymers with Different Cross-Linkers and Ion-Exchange Resins Exhibit Variable Adsorption of Anionic, Zwitterionic, and Nonionic PFASs, *Environ. Sci. Technol.*, 2020, **54**, 12693–12702.
53 C. Wu, M. J. Klemes, B. Trang, W. R. Dichtel and D. E. Helbling, Exploring the factors that influence the adsorption of anionic PFAS on conventional and emerging adsorbents in aquatic matrices, *Water Res.*, 2020, **182**, 115950.
54 J. Cao and F. Xiao, Interactions of per- and polyfluoroalkyl substances with polypropylene plastic and borosilicate glass: Resolving key uncertainties for accurate analysis, *J. Hazard. Mater. Adv.*, 2024, **16**, 100463.
55 C. E. Schaefer, G. M. Lavorgna, D. R. Lippincott, D. Nguyen, E. Christie, S. Shea, S. O'Hare, M. C. S. Lemes, C. P. Higgins and J. Field, A field study to assess the role of air-water interfacial sorption on PFAS leaching in an AFFF source area, *J. Contam. Hydrol.*, 2022, **248**, 104001.
56 G. Feng, B. Zhou, R. Yuan, S. Luo, N. Gai and H. Chen, Influence of soil composition and environmental factors on the adsorption of per- and polyfluoroalkyl substances: A review, *Sci. Total Environ.*, 2024, **925**, 171785.
57 H. Yang, Y. Zhang and S. Xia, Ferrihydrite/ultrasound activated peroxymonosulfate for humic acid removal, *Turk. J. Chem.*, 2022, **46**, 835–848.
58 C. T. Johnston and E. Tombácz, in *SSSA Book Series*, ed. J. B. Dixon and D. G. Schulze, Soil Science Society of America, Madison, WI, USA, 2018, pp. 37–67.

59 R. Zhang, W. Yan and C. Jing, Mechanistic study of PFOS adsorption on kaolinite and montmorillonite, *Colloids Surf., A*, 2014, **462**, 252–258.
60 F. Li, X. Fang, Z. Zhou, X. Liao, J. Zou, B. Yuan and W. Sun, Adsorption of perfluorinated acids onto soils: Kinetics, isotherms, and influences of soil properties, *Sci. Total Environ.*, 2019, **649**, 504–514.
61 Y. Ling, M. J. Klemes, S. Steinschneider, W. R. Dichtel and D. E. Helbling, QSARs to predict adsorption affinity of organic micropollutants for activated carbon and β-cyclodextrin polymer adsorbents, *Water Res.*, 2019, **154**, 217–226.
62 L. Axe and P. R. Anderson, Experimental and Theoretical Diffusivities of Cd and Sr in Hydrous Ferric Oxide, *J. Colloid Interface Sci.*, 1997, **185**, 436–448.
63 K. A. Barzen-Hanson, S. E. Davis, M. Kleber and J. A. Field, Sorption of Fluorotelomer Sulfonates, Fluorotelomer Sulfonamido Betaines, and a Fluorotelomer SulfonamidoAmine in National Foam Aqueous Film-Forming Foam to Soil, *Environ. Sci. Technol.*, 2017, **51**, 12394–12404.
64 Z. Du, S. Deng, Y. Bei, Q. Huang, B. Wang, J. Huang and G. Yu, Adsorption behavior and mechanism of perfluorinated compounds on various adsorbents—A review, *J. Hazard. Mater.*, 2014, **274**, 443–454.
65 M. S. Hellsing, S. Josefsson, A. V. Hughes and L. Ahrens, Sorption of perfluoroalkyl substances to two types of minerals, *Chemosphere*, 2016, **159**, 385–391.
66 Z.-W. Ke, S.-J. Wei, P. Shen, Y.-M. Chen and Y.-C. Li, Mechanism for the adsorption of Per- and polyfluoroalkyl substances on kaolinite: Molecular dynamics modeling, *Appl. Clay Sci.*, 2023, **232**, 106804.
67 S. E. Hearon, A. A. Orr, H. Moyer, M. Wang, P. Tamamis and T. D. Phillips, Montmorillonite clay-based sorbents decrease the bioavailability of per- and polyfluoroalkyl substances (PFAS) from soil and their transloca tion to plants, *Environ. Res.*, 2022, **205**, 112433.
68 Y. Zhi and J. Liu, Sorption and desorption of anionic, cationic and zwitterionic polyfluoroalkyl substances by soil organic matter and pyrogenic carbonaceous materials, *Chem. Eng. J.*, 2018, **346**, 682–691.